High-T_c Cuprate Superconductors: Materials, Structures and Properties

Anjela Koblischka-Veneva and Michael R. Koblischka

Abstract The cuprate superconductors are the first and the most important high-T_c superconducting materials, as still today applications of superconductivity at the temperature of liquid nitrogen (77 K) are only possible with cuprate superconductors (and here, especially the three compositions $YBa_2Cu_3O_{7-\delta}$ (abbreviated as Y-123 or YBCO), $Bi_2Sr_2CaCu_2O_{8+\delta}$ (Bi-2212) and $Bi_2Sr_2Ca_2Cu_2O_{10+\delta}$ (Bi-2223)). In this chapter, we present the crystal structures of the main 5 HTSc cuprate families (*Ln*-Cu–O (Ln-214), Y-Ba-Cu–O (YBCO), Bi-Sr-Ca-Cu–O (BSCCO), Tl-Ba-Ca-Cu–O (TlBCCO), and Hg-Ba-Ca-Cu–O (HgBCCO)) and their specific crystallographic features and discuss the resulting superconducting properties and the electric and magnetic characteristics being important for the applications, including the normal state properties, the grain boundary problem, the irreversibility lines, and issues of creating flux pinning sites to increase the critical current density, j_c. We further point out the progress in the material development in the direction for applications concerning the microstructure and texture and present the typical sample shapes.

Keywords High-T_c superconductors · Cuprates · Crystal structures · Phase diagram · Doping · Oxygen content · Irreversibility lines · Microstructure · Applications

1 Introduction

The cuprate high-temperature superconductors (HTSc) were the first materials with a superconducting transition temperature, T_c, above 30 K, being clearly above that of the previous record holder, Nb_3Ge films with $T_c = 23.2$ K [1–3]. In their pioneering paper, Bednorz and Müller (Nobel prize 1989) presented the compound LaBaCuO (the stoichiometric composition turned out to be $La_{1.85}Ba_{0.15}CuO_4$, now abbreviated as La-214) as a possible HTSc material [4]. The striking difference to all previous superconductors being metals and metal alloys was the fact that this material was a

A. Koblischka-Veneva (✉) · M. R. Koblischka
Experimental Physics, Saarland University, P.O. Box 151150, 66041 Saarbrücken, Germany
e-mail: a.koblischka@gmail.com

Y. Slimani and E. Hannachi (eds.), *Superconducting Materials*,
https://doi.org/10.1007/978-981-19-1211-5_7

ceramic, which was thought to be impossible as ceramics are normally insulators. Soon after the results could be reproduced by other groups, a race for even higher T_c's set in, the early stages of which are nicely narrated in the book by Hazen [5] and in very short times after, the compound $(La,Sr)_2CuO_4$ was found with $T_c = 38$ K [6]. By high-pressure experiments on La-Ba-Cu–O, the idea came up to replace La by the smaller ion of Y, and so the YBCO compound with a T_c of 91…93 K was found by Wu et al. [7] and Chu et al. [8]. This was the first time to raise T_c above the temperature of liquid nitrogen (77 K), so superconductivity was no longer a phenomenon which could take place only behind the steel walls of cryostats, but could now be demonstrated easily to the public or even in class rooms. Following this progress, about a year later the first members of the BSCCO-family were announced by Maeda et al. [9] and Zandbergen et al. [10], raising T_c from 85 K in $Bi_2Sr_2CaCu_2O_{8+\delta}$ (Bi-2212) to 105 K in $Bi_2Sr_2Ca_2Cu_3O_{10+\delta}$ (Bi-2223). The next steps of the quest to find materials with even higher T_c were the finding of the Tl-based superconducting family [11–13] and the Hg-based family [14, 15], which brought up T_c to 138 K in slightly Tl-doped $HgSr_2Ca_2Cu_3O_9$ (Hg-1223). This material still holds today the T_c record for a material in ambient conditions [1]. Under pressure, the T_c of Hg-1223 could be raised further to 165 K [16, 17], which is now surpassed by reaching nearly room temperature in H_3S [18] and then in LaH_{10} [19]. Even though now more than 100 HTSc superconductors are known with T_c's above the HTSc limit of 30 K, none of these materials could further improve the maximum T_c [20]. The main HTSc families and their maximum T_c are plotted in Figs. 1 and 2 below.

The La-124 system was developed further with family members doped with electrons, instead of hole-doping like for all other cuprate HTSc, making up the general

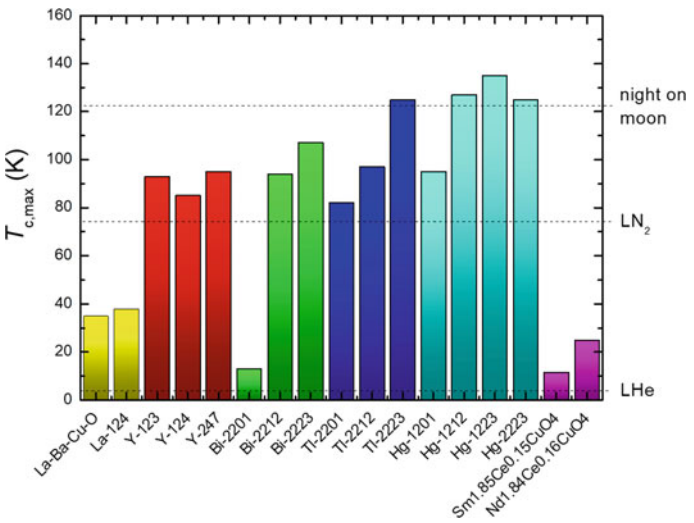

Fig. 1 Superconducting transition temperature, T_c, of various cuprate HTSc. Different HTSc families are indicated by different colors. Data were collected from Refs. [1–3]

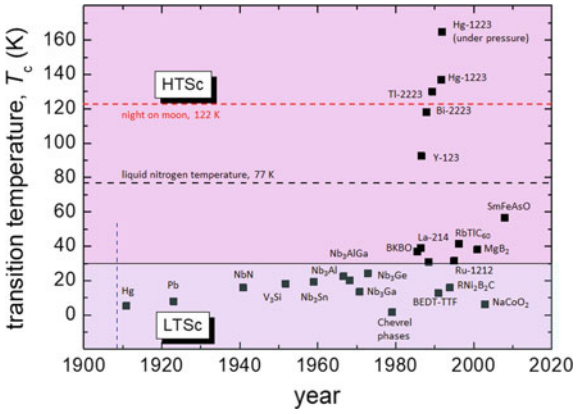

Fig. 2 The raise of T_c as a function of time, starting from the first superconductor, Hg, discovered in 1911. The borderline between LTSc and HTSc is defined at $T = 30$ K, and several other superconducting materials discovered since 1960 are also shown for comparison. Data were collected from Refs. [1–3]

formula $Ln_{2-x}M_xCuO_{4-\delta}$ (with Ln = rare earths Pr^{3+}, Nd^{3+}, Sm^{3+}, or Eu^{3+} and M = Ce^{4+} or Th^{4+} where $x \approx 0.1$–0.18 and $\delta \approx 0.02$), yielding the highest T_c of about 25 K for NCCO (i.e. $Nd_{2-x}Ce_xCuO_{4-\delta}$) [21, 22]. These materials are especially important to test theories of the Cooper pair formation in HTSc materials.

From the applications' point of view, only the three systems, (*RE*)-BCO with *RE* denoting light rare earth elements, i.e., Nd, Eu, Sm and Gd, and the Bi-2212 and Bi-2223 systems, are really useful materials to be produced in a variety of shapes, ranging from epitaxial thin films, thick films, coated conductors, powder-in-tube wires and tapes, and bulk materials [23–25]. Very recently, even superconducting foams [26, 27] and nanofiber mats [28, 29] could be produced. Most attractive for many applications are such with cooling by liquid nitrogen ($T = 77$ K), even though nowadays the development of cryocooling systems [30] has largely advanced allowing to reach even low temperatures in a cryogen-free manner.

Figure 2 gives the superconducting transition temperatures, T_c, as function of the year of discovery, starting from 1911 with Hg discovered by Kammerlingh Onnes [31]. A borderline at 30 K separates the conventional, low-T_c superconductors (LTSc) from the HTSc compounds [1].

The common feature of all the cuprate HTSc crystal structures is the layered structure consisting of several different plane layers. The most important one are the Cu–O-planes, which are considered to be the main superconducting highways. All other layers in the crystal structure serve as charge carrier reservoirs. The layered structure leads in turn to a high anisotropy of the superconducting properties [1–3], which causes interesting magnetic properties as discussed in Chap. 3. Another common issue for all cuprate superconductors is the fact that they are ceramic oxidic materials, and as consequence, the oxygen loading and oxygen distribution within the Cu–O-planes is an important issue for the resulting superconducting performance. A generic phase diagram of the HTSc materials is presented in Fig. 3 below. Depending on the hole concentration p, the material can be driven from an antiferromagnet (AF, with the corresponding Néel temperature T_N) via a spin glass state to a superconductor, SC.

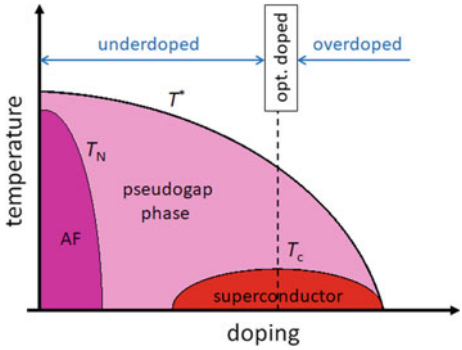

Fig. 3 Generic phase diagram for cuprate HTSc showing temperature versus the charge carrier concentration (doping)

At temperatures above T_N or T_c, the compound may behave as "normal" metal, mostly as semiconductor [32, 33]. This coexistence of an antiferromagnetic state with superconductivity may be the key for the underlying pairing mechanism in the cuprate HTSc [34].

In this chapter, we discuss the crystal structures of the cuprate HTSc families and the resulting consequences, the microstructures and the important superconducting properties. Furthermore, we discuss the use of the cuprate HTSc in applications of superconductivity.

2 Crystal Structures of the Cuprate HTSc Families

The HTSc cuprate superconductors have either tetragonal or orthorhombic crystal structures, and their unit cells are formed by stacking various layers together along the *c*-direction, which causes the *c*-axis parameter to be much longer than the *a*- and *b*-axes. One or more Cu–O-planes that are present are particularly important, as they constitute the superconducting layers, where the mobile charge carriers (electrons or holes) reside and that undergo superconducting condensation when cooled below T_c. Other intervening metal oxide and pure metal layers are present as well, namely Tl–O, Bi–O, Hg–O, Ba–O, and Sr–O layers. Furthermore, Cu–O chains, and Y and Ca layers appear in the HTSc unit cells, which provide the necessary structural framework for the pertinent number of Cu–O-planes to exist. Several of the oxide layers (e.g., Tl–O, Bi–O, Hg–O layers and the Cu–O chains) exhibit a mixed-valence character, which makes them serve as charge reservoir layers supplying mobile carriers to the superconducting Cu–O-planes. At the same time, these layers render a low dimensionality to their electronic structure by serving as blocking or spacer layers between the superconducting layers. A negative consequence of the presence of such additional layers is that they weaken the electronic coupling along the *c*-direction to make the material quasi-two-dimensional, and thus promote a significant anisotropy in both the superconducting and normal states. The ratio of the normal-state resistivities along and perpendicular to the *c*-direction, ρ_c/ρ_{ab}, ranges from the order of 10^2

to the order of 10^5 and the critical current across the layers in the superconducting state can be orders of magnitude lower than in the (*a*,*b*)-plane [20, 35]. This poses a serious constraint and a challenge for material science to prepare HTSc conductors achieving the high critical current densities, j_c, required for practical applications [36].

2.1 YBCO

We will start with the YBCO compound, which is the most important HTSc material for present-day's applications [23–25]. Interestingly enough, YBCO was the first HTSc material with T_c at 91 K, which is well above 77 K, the temperature of liquid nitrogen, allowing the operation of applications at this temperature. Starting from high pressure studies on LBCO, Chu et al. [8] noted a large and positive pressure coefficient of T_c, with the onset of superconductivity occurring at 52.5 K [37]. So, the idea was born to simulate this pressure in a chemical way (i.e., internal pressure) by replacing La^{3+} with the smaller Y^{3+} ion. The resulting material was a mixture of two phases, the superconducting (black) YBCO and the green (insulating) Y_2BaCuO_5 (Y-211) phase [5]. This phase mixture is still an important issue to create a reasonable amount of flux pinning sites in the 123-compounds today [38].

The unit cell of $YBaCuO_{6+y}$ possesses double Cu–O-planes and a single plane with Cu–O-chains as shown in Fig. 4 for $y = 0.5$ (double unit cell), $y = 0.7$ and $y = 1.0$. YBCO has an orthorhombic unit cell (i.e., $a \neq b$) for $y = 0.5$ to 1.0, and a tetragonal one ($a = b$) below 0.5. The material is optimally doped at $y = 1.0$ (that is, O_7), and is underdoped for all other y [39–41]. This is further illustrated in Fig. 5

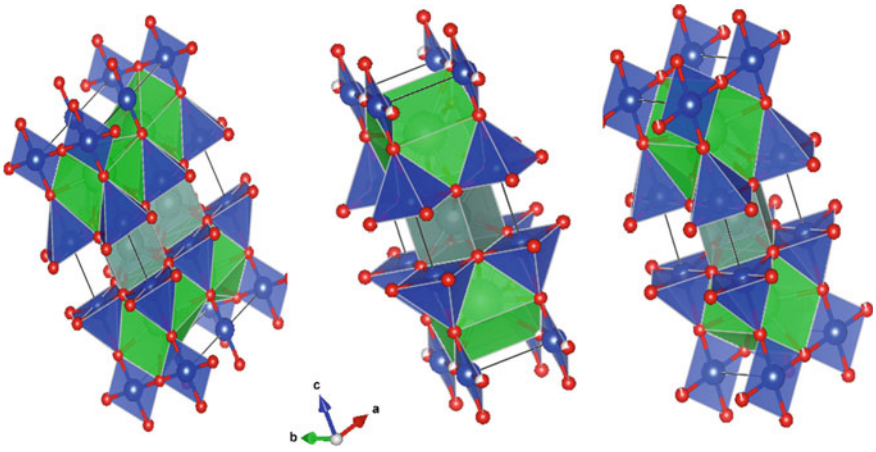

Fig. 4 Crystal structures of YBCO compounds depending on the oxygen content, *y*, ranging from $y = 0.5$ (half doped) via $y = 0.7$ (underdoped) to $y = 1.0$ (optimally doped)

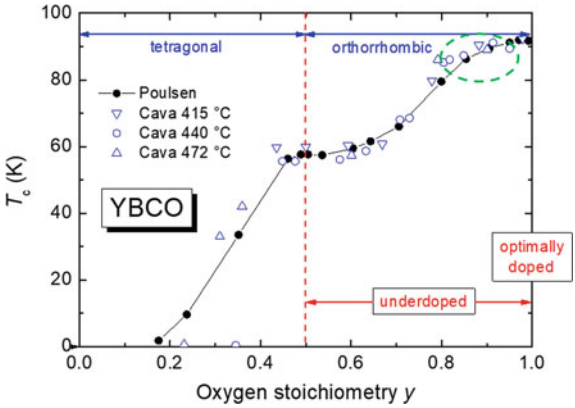

Fig. 5 T_c as function of the oxygen content (redrawn with permission from Ref. [40]). Below $y = 0.5$, YBCO is tetragonal, above orthorhombic. YBCO is optimally doped at $y = 1$, otherwise only underdoped. The green circle marks the range where δT_c-pinning can appear (fishtail effect in the MHLs)

below. Practically, to reach full oxygen loading, long times are required (diffusion), so this poses a problem when fabricating large sample sizes like YBCO bulks [42]. Note also that it is not possible to create an overdoped YBCO superconductor by oxygen loading.

The consequence of all this is a strong dependence of YBCO on the oxygen loading achieved. In [40], Poulsen et al. have shown by experimental neutron scattering data and simulations that the oxygen atoms have a strong tendency to form chains in the Cu–O-planes. In the state $y = 0.5$, every second row of oxygen atoms is unoccupied, thus the doubling of the unit cell to describe this situation properly. A slight oxygen deficiency is already sufficient to reduce T_c, which poses a big problem when investigating the surface of an YBCO crystal under UHV conditions, e.g., by STM [43, 44]. For $y < 1$, regions with lower T_c (= broken chains) are embedded in the $YBCO_7$ matrix when being close to optimal doping. If these regions are of similar size to ξ, then the order parameter only varies slightly, but if the regions are larger than $2\,\xi$, so-called δT_c-pinning sites [45, 46] may be formed, and the corresponding magnetization loops may show the so-called fishtail effect [45, 47]. The resulting fishtail effect is only weak, and further oxygen loading may completely remove this peculiar shape of the MHLs again in ultrapure single crystals [48]. The region, where this can happen, is marked by the green dashed circle in Fig. 5 below. In this sense, an YBCO crystal with $y < 1$ can be seen as a granular material on the nanoscale, which confirms the early observations of Däumling et al. [49].

In subsequent experiments, it was soon realized that the formation of the high-T_c phase was not confined to Y^{3+} alone, but, a superconducting *RE*-123 family could be created [50] with nearly all lanthanides *RE*, except Ce and Tb, resulting in non-superconducting multi-phases. This is commonly attributed to their relatively bigger ion size (see also Fig. 6). The case of Pr was long debated in the literature, but the final conclusion is that also Pr does not yield a superconducting material [51, 52].

Figure 6 presents the lattice parameter of the *RE*-BCO unit cells for the rare earth elements in the order of their ionic radius, compiled from literature data. Erbe et al. [53] also showed recently the lattice parameter of the two most important

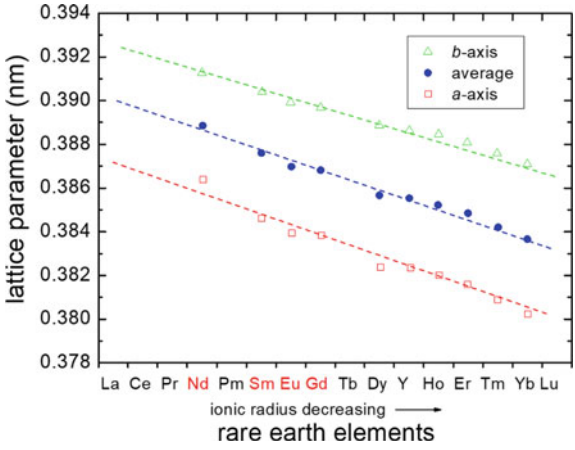

Fig. 6 Lattice parameter of RE-BCO depending on the ionic radius of the RE ions, (data were collected from Ref. [53]). The four *LRE* elements are marked in red. Pr, Tb and Ce do not form HTSc materials, Pm is radioactive

substrates for thin film production, $SrTiO_3$ (STO) and $LaAlO_x$ (LAO), which are just engulfing the *RE*-BCO compounds, thus leading to some stress/strain in the thin film samples. The quest to further enhance the critical currents in the *RE*-BCO compounds, especially for large bulk samples, lead to interesting combinations of more than one *RE* element, leading to binary [54, 55], ternary [56, 57], and even to HEA-inspired (see Chap. 6) *RE*-BCO compounds with five *RE* elements [58], where the increased disorder on the Y-site provides new possibilities to design an appropriate material for applications with high current densities.

For the set of light rare earth elements (*LRE* = Nd, Sm, Eu and Gd), the ion size of the LRE^{3+}-ion becomes comparable to that of Ba^{2+}-ion. As result, the LRE^{3+}-ion can substitute Ba^{2+}, thus forming a *LRE*-rich compound with reduced superconducting properties (T_c ~ 65 K) [59]. A controlled mixture of these two phases by dedicated processing steps enables increased flux pinning, at low temperatures by variation of the order parameter ξ (δT_c-pinning) and at elevated temperatures by magnetic-field induced pinning of the *LRE*-rich sites rendered normal. The final result are magnetization curves with a large secondary peak, i.e., strongly increased critical currents at elevated magnetic fields [46, 60]. In contrast to the fishtail effect caused by oxygen vacancies, this *LRE*-induced fishtail effect is very strong and also not reversible. All these observations nicely illustrate the importance of nanoengineering of flux pinning sites in the *RE*-BCO compounds to tailor the flux pinning properties and the resulting critical current densities [61].

The surface of NdBCO is reported to be much more stable as that of YBCO, so measurements within an UHV environment are possible [63]. Low-temperature scanning tunnelling spectroscopy (STS) was performed on high-quality, doped Nd-123 single-crystal samples [62] as shown in Fig. 7 with T_c values of 76 K (highly underdoped), 93.5 K (underdoped) and 95.5 K (optimally doped), respectively. The measurements were taken on an (*a*, *b*)-plane for the underdoped samples and on a (*b*, *c*)-plane for the optimally doped sample. From the d*I*/d*V*-curves obtained showing features like the conductance peaks (marked as P), dips (D) and humps (H), the

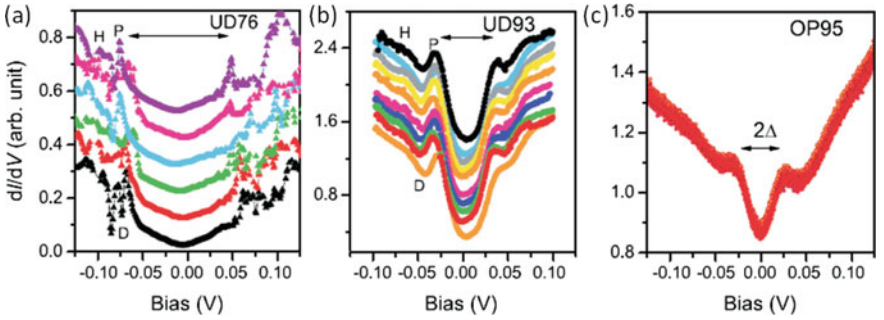

Fig. 7 Representative dI/dV-curves obtained at $T = 4.2$ K on NdBCO single crystals with T_c values of 76 K (highly underdoped, UD76, **a**), 93.5 **K** (underdoped, UD93, **b**) and 95.5 **K** (optimally doped, OP95, **c**). Spectra shown for UD76 were obtained along a 5 nm scan line and for UD93 they were obtained along a 20 nm scan line. The spectra shown for OP95 were obtained at the same location. The curves observed at different locations are staggered for clarity. Reproduced with permission from Ref. [62]

energy gap (2Δ) measured from peak-to-peak separation monotonically increases as the T_c values decrease monotonically due to underdoping. In detail, values of 56 ± 4 meV for OP95, 70.6 ± 1.5 meV for UD93 and 117 ± 25 meV for UD76 were obtained. These values are in the range reported for both Bi-2212 and YBCO compounds [64].

The YBCO-family has two more members by created by adding additional layers to the original composition. The compound $RE\mathrm{Ba_2Cu_4O_8}$ (i.e., *RE*-124, where *RE* denotes any lanthanide other than Ce, Tb, or Pr) with $T_c \sim 80$ K was subsequently discovered, which is an analogue of *RE*-123, but with an extra plane containing Cu–O chains [65], whereas a combination of the 123 and 124 systems turned out to be an ordered inter-growth in the form of the $\mathrm{Y_2Ba_4Cu_7O_{15}}$ (Y-247) system, which has a T_c of 95 K [66]. The crystal structures of Y-124 and Y-247 are presented in Fig. 8. Y-124 was found to appear as stacking fault in Y-123 crystals. The more complicated preparation route to achieve pure materials has excluded them from applications.

2.2 BSCCO Family

Starting from the LaSrCuO compound, Michel et al. [67] had found the T_c of several Bi–Sr–Cu–O compounds to range between 7 and 22 K, which later was raised even to 34 K. These findings suggested the replacement of the La-ion by Bi in LSCO, although the resulting crystal structure was found to be different from the original $\mathrm{K_2NiF_4}$ structure. The crystal structures of the BSCCO family are illustrated in Fig. 9, starting with the single CuO-layer ($n = 1$) compound $\mathrm{Bi_2Sr_2CuO_6}$ (Bi-2201), having a T_c of ~25 K. Subsequently Maeda et al. [9] found a substantially enhanced T_c of the order of 80–110 $_K$ for Bi–Sr–Ca–Cu–O (BSCCO), and the generic formula of

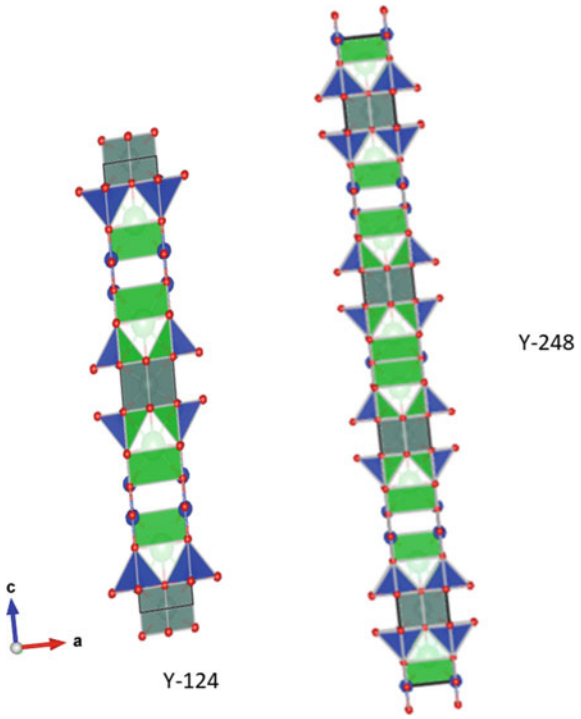

Fig. 8 Crystal structures of the YBCO-family members, Y-124 and Y-247. Y-124 has an extra chain layer as compared to Y-123, and Y-247 is an intergrowth of both Y-123 and Y-124 phases

the BSCCO family turned out as $Bi_2Sr_2Ca_{n-1}Cu_nO_{2n+4}$. For the $Bi_2Sr_2CaCu_2O_{8+d}$ (Bi-2212) compound with two (n = 2) Cu–O-layers, T_c ranged from 85 to 95 K, while for $Bi_2Sr_2Ca_2Cu_3O_{10+d}$ (Bi-2223) containing three (n = 3) Cu–O-planes, T_c was up to 110 K [10]. A partial substitution of Bi by Pb, $(Bi,Pb)_2Sr_2Ca_2Cu_3O_{10+d}$, was found to contribute to the phase stability in the processing steps [68]. Among the BSCCO family, the Bi-2212 compound has the highest anisotropy, which is the highest one of all HTSc compounds [20]. This leads, of course, to interesting consequences concerning the magnetic properties as discussed in Chap. 3.

Many of the superconducting and normal state properties of the BSCCO compounds were discussed in [70]. Important is here that in the BSCCO system underdoped, optimally doped and overdoped superconductors may be created, which enables to test the prediction of the phase diagram. Figure 10 illustrates how the resistivity curves will vary upon doping for the two situations, in-plane and out-of-plane. Thus, one can recognize, e.g., the optimally-doped situation directly from the resistivity measurement.

Figure 11 presents resistivity measurements carried out on optimally doped Bi-2212 as well as on underdoped material [71, 72]. The resistivity curve of the underdoped material is assumed to approach the pseudogap temperature, T^*, visualized by the first deviation from the otherwise linear behavior.

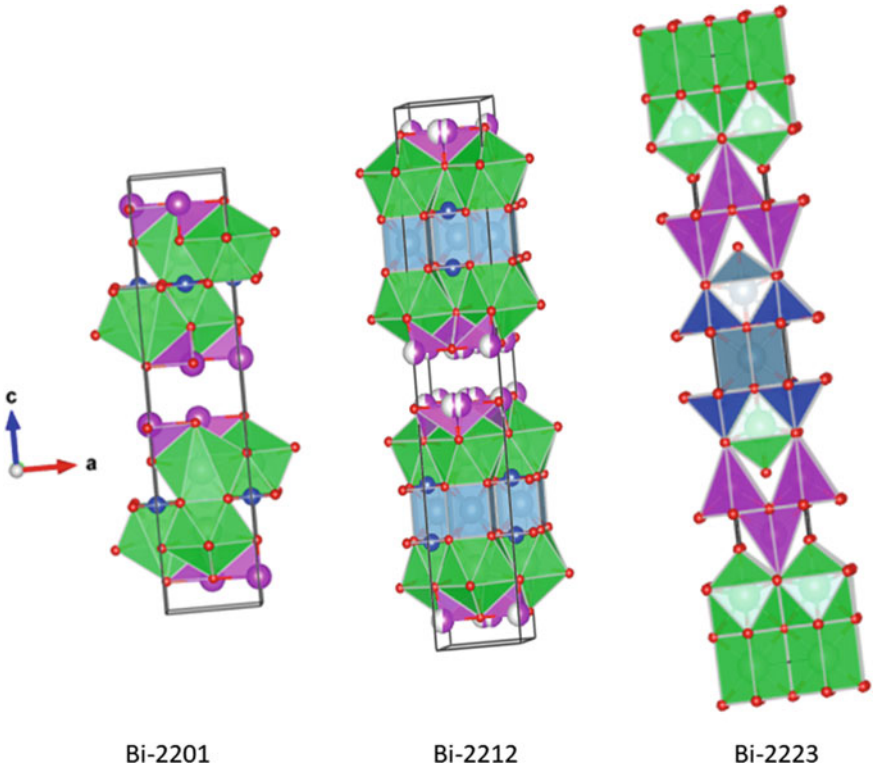

Fig. 9 Crystal structures of members of the BSCCO HTSc family, Bi-2201, Bi-2212 and Bi-2223

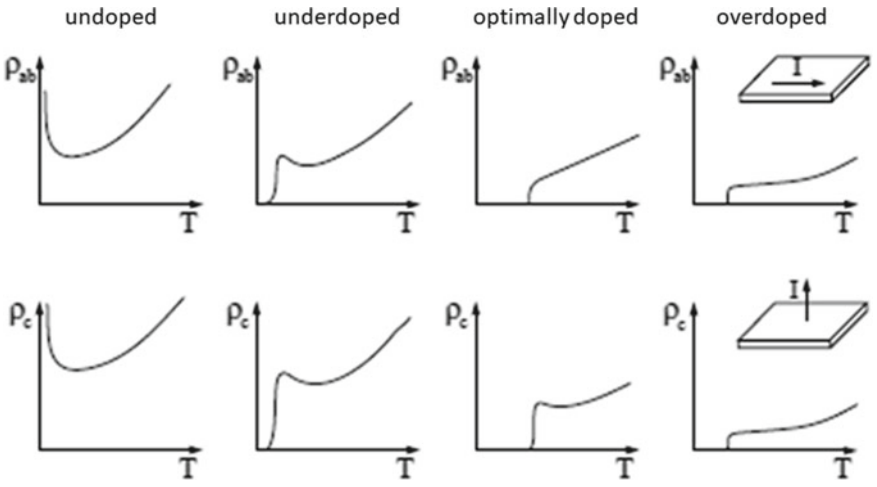

Fig. 10 Schematic overview of the dependence of the measured resistivity on doping effects. The top row shows the in-plane resistivity, and the lower row the out-of-plane resistivity. The two insets illustrate the direction of the current, *I*. Reproduced with permission from Ref. [69]

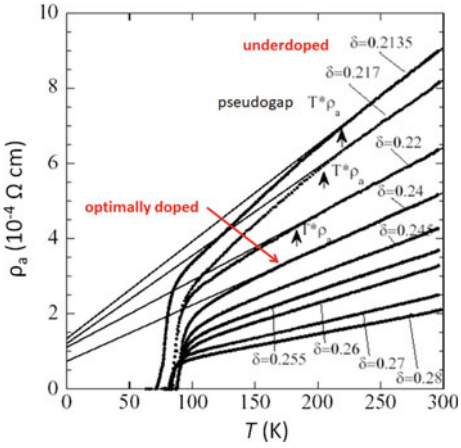

Fig. 11 Resistivities along the *a*-axis measured on Bi-2212 single crystals for various oxygen dopings, δ. Optimally doped material ($\delta = 0.24$) shows no extra kink at high T indicating the pseudogap temperature T^* (see also the phase diagrams), whereas underdoped material ($\delta = 0.22$–0.2135) does. Reproduced from Ref. [72]

Furthermore, the BSCCO material is less sensitive to oxygen loss, so proper surfaces may be prepared by cleaving under UHV conditions, so high-resolution STM measurements became possible especially on the Bi-2212 system, revealing interesting physics. Figure 12 shows two so-called gap-maps as determined by STM/STS [73], where the superconducting gap is determined from I/V-curves measured locally by STS (see also Fig. 7) and then plotted as a function of position. These maps reveal the local variation of the superconducting gap size, and it is clearly visible that regions with similar gap sizes form clusters in both cases (a—underdoped) and (b—as grown, which is slightly overdoped). As seen before in the case of NdBCO, the

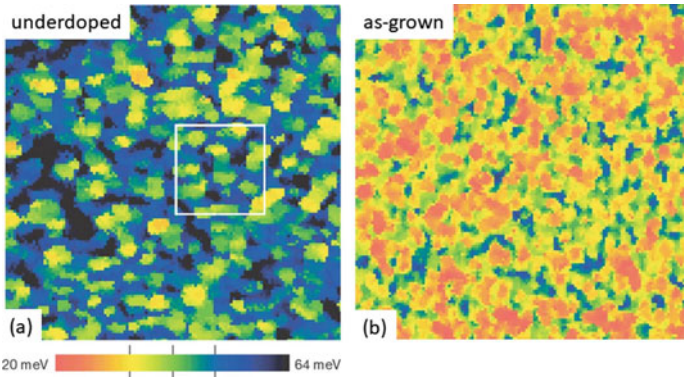

Fig. 12 STM images ("gap maps") of a Bi-2212 single crystal. **a** Shows an underdoped crystal, and **b** the as-grown state (which is, i.e., slightly overdoped). The color code for the superconducting gap is chosen to be the same for both images. The observation temperature was $T = 4.2$ K; the image size is 56×56 nm^2. The points in the white rectangle were further analyzed in [63]. Note that the gaps in (**a**) and (**b**) are quite different from each other, but in both cases, nanometer-sized areas of different gaps are visible in the images. Reproduced with permission from Ref. [73]

superconducting gaps of the underdoped samples are much larger as compared to the optimally doped or overdoped cases, the two maps differ in the size of the measured gaps, but show the same clustering.

The gap maps clearly demonstrate that oxygenation is creating a kind of internal granularity (i.e., a spatial variation of the superconducting gaps due to different oxygen content) on the nanometer scale even in high-quality single crystals. This important result should always be kept in mind when interpreting results of electric or magnetic measurements of superconducting properties of HTSc samples.

2.3 TlBCCO Family

By completely replacing Bi by Tl and Sr by Ba, that is, forming the Tl–Ba–Ca–Cu–O family (in short TBCCO), one may have single- or double-Tl-layered compounds [11] with the generic chemical compositions $TlBa_2Ca_{n-1}Cu_nO_{2n+3}$ and $Tl_2Ba_2Ca_{n-1}Cu_nO_{2n+4}$, respectively. Crystal structures of the compounds Tl-1212, Tl-1223 and Tl-2212 are presented in Fig. 13.

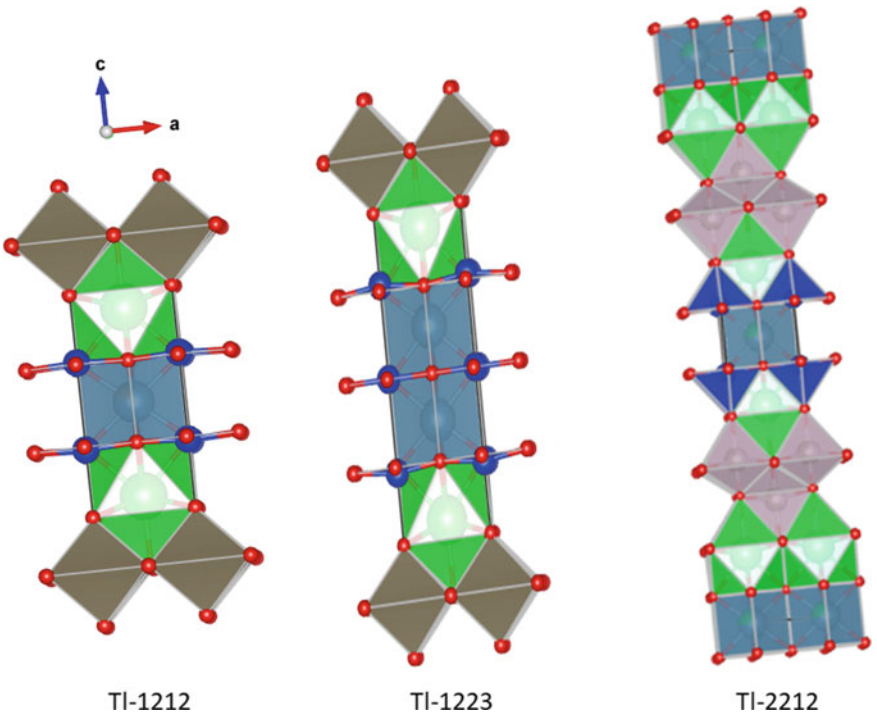

Fig. 13 Crystal structures of the Tl-based HTSC family, showing the compounds Tl-1212, Tl-1223 and Tl-2212

As already seen in case of the BSCCO compounds, the nominal composition and the processing schedule influence the resulting T_c and the structural details of the synthesized phases of the TBCCO system. Most notable is here that among the single-Tl-layer compounds, Tl-1223 and Tl-1234 exhibit the highest T_c values of 133 K [12] and 127 K [74], respectively. Among the double-Tl-layer compounds, the two compositions Tl-2223 and Tl-2234 possess T_c values of 128 K [13] and 119 K [75], respectively. The structural, chemical and mechanical properties of the TlBCCO family were summarized by Bellingeri and Flükiger [76], including also the less common members of the family like Tl-1222, Tl-1234 and Tl-2234. The last two compounds exhibit even four Cu–O-layers per unit cell. The pressure dependence of T_c of the two compounds Tl-2223 (3 Cu–O-layers) and Tl-2234 exhibited a clear kink at ~12 GPa [12], suggesting that the inner and outer Cu–O-layers, which are inequivalent (the inner layer has fourfold oxygen coordination, the outer ones fivefold), also behave differently under pressure. In ambient conditions, due to the only proximity weak coupling between the Cu–O-layers, T_c is determined by the Cu–O-layer with the highest intrinsic T_c.

Due to the high T_c and the lower anisotropy as compared to Bi-2212, it was attempted to fabricate powder-in-tube tapes, especially with the compound Tl-1223, which presented reasonably high irreversibility fields. However, the grain boundary weak link problem, which is essential for all HTSc compounds [77–79], led only to reduced critical current densities of these tapes [80], making them obsolete for applications. Furthermore, the compounds Tl-1212 and Tl-2212 were used for the fabrication of microwave devices, showing a low surface resistance in frequencies up to 10 GHz [81]. Another important obstacle is the toxicity and volatility of Tl, which is according to [76] controllable by taking specific measures and encapsulating the superconducting material like as is done in the Ag-sheathed tapes. However, extra costs caused by these procedures are hindering the applications of the TlBCCO compounds.

2.4 HgSCCO Family

The HgSCCO HTSc family is rich of members following the basic compositions $HgBa_2Ca_{n-1}Cu_nO_{2n+3}$ and $Hg_2Ba_2Ca_{n-1}Cu_nO_{2n+4}$ [14–16] describing single- and double-layered Hg systems. Figure 14 presents the crystal structures of the Hg-1201, Hg-1212 and Hg-1223 compounds. As pointed out already before, the single-Hg-layered compound Hg-1223 exhibiting three Cu–O planes (n = 3) has a T_c of 134 K, but has manifested the highest $T_c = 138$ K of all cuprate HTSc, when Hg is marginally replaced by 0.2% Tl. Now other material showed a higher T_c at ambient conditions, even to date.

Schwartz and Sastry [82] summarized the properties of the HgBCCO family members, and also the efforts made with the fabrication of thin films, thick films and tapes of the Hg-based compounds. Although the irreversibility lines of the undoped

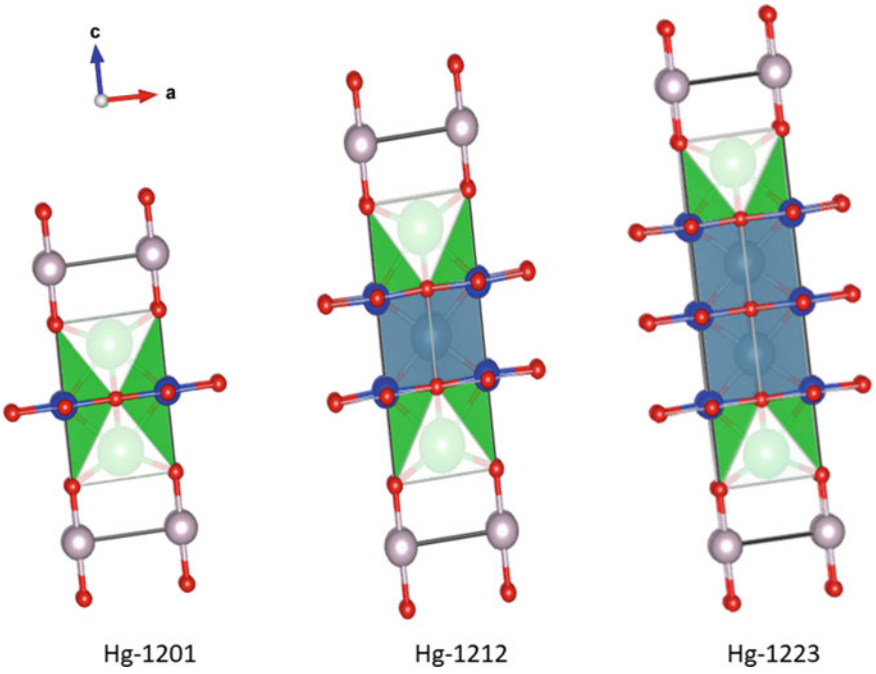

Fig. 14 Crystal structures of the Hg-based HTSC family, showing the compounds Hg-1201, Hg-1212 and Hg-1223, the T_c-record holder for the cuprate HTSc

and doped $HgBa_2Ca_{n-1}Cu_nO_{2n+2}$ compounds show the highest values for the irreversibility field at high temperatures of any known superconductor, it is only comparable to that of YBCO at 77 K. Furthermore, it was found that the position of $B_{irr}(T)$ is strongly dependent upon added dopants, which is an important issue from both fundamental and technological points-of-view, offering possibilities to tailor the magnetic properties.

Plotting the irreversibility field, B_{irr}, versus the reduced temperature, T/T_c, it was shown that B_{irr} is above that of the Bi–Sr–Ca–Cu–O double layer compounds, but below the one of the YBCO compound [83]. This observation is thus consistent with the model that the irreversibility field as a function of normalized temperature is inversely proportional to the separation of the Cu–O-layer in the unit cell. As a consequence of the record-high T_c, the absolute value of $B_{irr}(T)$ is as high as that of YBCO at 77 K, and consequently, above it for higher temperatures [84].

There have been several efforts in the literature to produce especially thin film materials of the HgBCCO family members, but overall, the fact that HgBCCO materials are not considered for practical applications demonstrates that T_c is not the decisive criterion for the use in applications, but the achievable critical current density, j_c.

Figure 15 shows the superconducting transition temperature, T_c, as a function of n, the number of Cu–O-layers per unit cell for the BSCCO, TlBCCO and HgBCCO

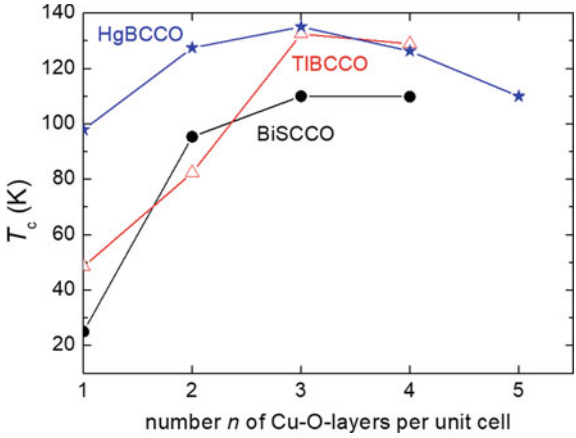

Fig. 15 T_c as function of the layer number n of Cu–O-layers per unit cell of the BSCCO, TlBCCO and HgBCCO HTSc families. Data were collected from Ref. [85]

families. The highest T_c's are obtained at n = 3, whereas an increase to 4 Cu–O-layers reduces T_c again, which is also a consequence of the inequality of the inner and outer Cu–O-layers as observed in the pressure experiments [12]. Nevertheless, it was attempted to create a so-called infinite layer compound, $(Sr_{1-x}Ca_x)_{1-y}CuO_2$, consisting of only Cu–O-layers in the literature, but the resulting T_c reached in first experiments hardly 45 K, but was reported to achieve 110 K in later experiments [86]. The fact that the infinite layer compound does not achieve a very high T_c proves the importance of the charge carrier reservoirs and spacer layers for the high-T_c superconductivity in the other cuprate HTSc materials.

2.5 RE-*214 Family*

The general formula of the *RE*-214 family is $La_{2-x}M_xCuO_4$ (M = Ba, Sr, Ca, or Na; with x = 0.15–0.17). This family was developed on the base of the first experiments by Bednorz and Müller [4], reaching a maximum T_c value of 38 K [6]. However, this was only the start of this HTSc family, which developed further into the most complete HTSc family with both hole-doped and electron-doped members. As the basic pairing mechanism for high-T_c superconductivity is still unknown, the common opinion is that the Cu–O-planes play the key role, and these planes can be obtained by electron- or hole doping of the parent Mott insulator system. Thus, the finding in 1989 of true electron superconductors among the cuprate HTSc has significant implications for the understanding of HTSc superconductivity, allowing to test new and existing theories experimentally [21, 87, 88]. The first electron-doped analogue of the LSCO cuprate system was $RE_{2-x}M_xCuO_{4-\delta}$ (*RE* = rare earth elements Pr^{3+}, Nd^{3+}, Sm^{3+}, or Eu^{3+}; and $M = Ce^{4+}$ or Th^{4+}; with the parameters $x \approx 0.1$–0.18 and $\delta \approx 0.02$). The highest T_c of this group was 25 K for the NCCO compound (i.e., $Nd_{2-x}Ce_xCuO_{4-\delta}$).

The electron-doped cuprate family does have the Cu–O-planes like the other cuprate HTSc, but the oxygen coordination is different. Figure 16 presents the crystal structure of NCCO (called T'-phase) in comparison with the other crystal structures (T-phase showing Cu–O octahedra) and the T*-phase (showing Cu–O pyramids). While the hole-doped HTSc are either of the T or the T*-phase type, the T'-phase is composed of sheets of Cu–O squares and has no apical oxygen atoms. As result, the T'-phase can only be doped by electrons [89]. Figure 17 gives the phase diagram for the *RE*-214 family, which is the most complete one of all cuprate HTSc families. There are two superconducting domes (SC) on each side of the diagram, separated by the antiferromagnetic (AF) phase. The resulting T_c values of the NCCO compounds are ranging only between 13 and 25 K, while the highest T_c of LaCCO of 30 K can only be stabilized in thin film form. These low T_c's do not pose a problem for the basic research, but there are no envisaged applications of this cuprate HTSc family to date.

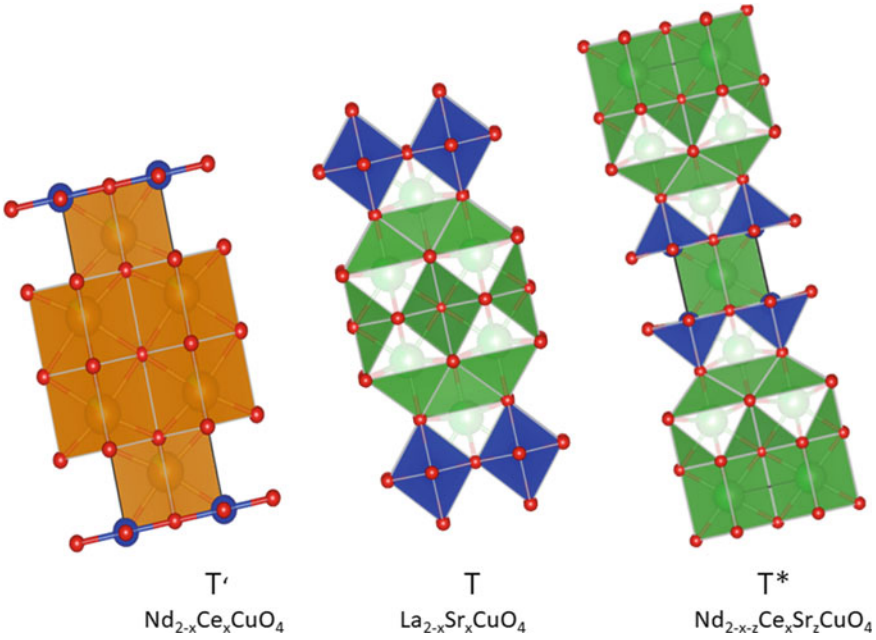

Fig. 16 Crystal structures of the 214 HTSc family with the three compounds $Nd_{2-x}Ce_xCuO_4$ (T'), $La_{2-x}Sr_xCuO_4$ (T) and $Nd_{2-x}Ce_xSr_2CuO_4$ (T*)

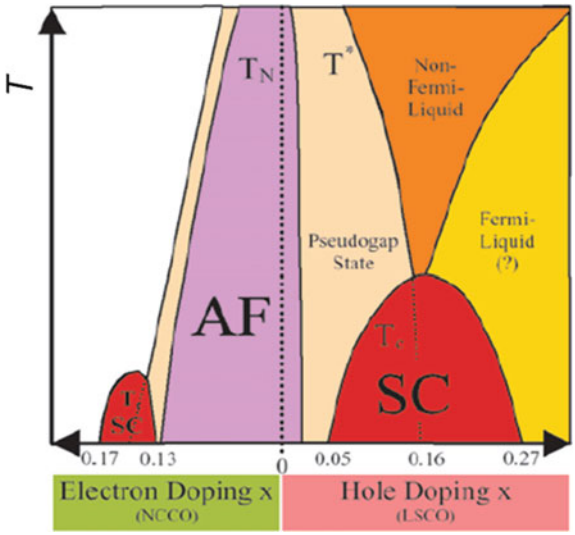

Fig. 17 Phase diagram of the *RE*-214 HTSc family with both hole-doping and electron doping. Superconducting states are obtained in the two red domes on both sides of the diagram, separated by the antiferromagnetic state. Reproduced with permission from Ref. [88]

3 Important Superconducting Properties and Typical Microstructures

The most important property for applications of superconductors is the achievable critical magnetic fields as those define in which fields the superconductor stays superconducting. However, as discussed in Chap. 3, the irreversibility fields are the ones limiting the superconducting performance of the HTSc materials. Thus, Fig. 18 presents the irreversibility fields, $B_{irr}(T)$, together with the $B_{c2}(T)$-lines for various HTSc materials. The $B_{irr}(T)$-line or often called irreversibility line (IL) gives the upper limit for possible applications as the flux pinning, and thus the critical currents, goes to zero at this line, but the material stays superconducting up to the upper critical field, $B_{c2}(T)$. The data presented are collected from various literature data [90, 91]. Here, one should note that the IL is always located much lower than the corresponding $B_{c2}(T)$, which is due to thermally activated flux creep, and the principal temperature dependence of both lines is supposed to be similar [45]. An exception to this rule occurs if there are anisotropy effects present, i.e., the rigid vortex lines are dissociating into vortex pancakes which only exist within the Cu–O-planes [92]. In this case, the temperature dependencies of the vortex state and the pancake state can be clearly different from each other, whereby the low temperature part corresponds to the ones of the less anisotropic samples.

This is, e.g., realized in the case of Bi-2212, where a clear change of shape of the IL below 20 K is visible in the diagram [91]. The effect is less pronounced in Bi-2223, which is accordingly also less anisotropic than Bi-2212. The $B_{c2}(T)$-lines of both materials are not shown, but $B_{c2}(T)$ of Bi-2212 is almost similar to that of YBCO but reaching even higher fields at low T, so there is a hugh differences between

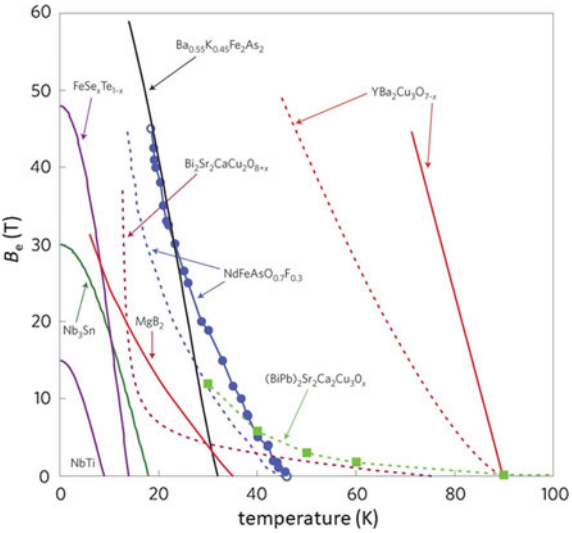

Fig. 18 Diagram comparing the irreversibility fields, B_{irr}(T) and the upper critical fields, $B_{c2}(T)$, of various HTSc materials. The conventional LTSc alloys NbTi, Nb_3Sn and MgB_2 are also included for comparison, and also $NdFeAs_{0.7}F_{0.3}$ and $FeSe_{1-x}Te_x$, which are two different types of iron-based superconductors. The full lines indicate the $B_{c2}(T)$-lines of a superconductor, and the dashed lines represent the irreversibility lines. Note the difference between $B_{c2}(T)$ and $B_{irr}(T)$ of Y-123, which reflects the effect of thermal fluctuations. The BSCCO materials show the effect of dimensionality. Reproduced with permission from Ref. [90]

the two lines. The ILs strongly depend on the experimental conditions, that is, the sweep rate of the external magnetic field or the current criterion employed in the measurements due to the thermally activated flux creep. Therefore, an analysis of the underlying pinning mechanism(s) by only measuring the IL is not straightforward. Table 1 presents the superconducting parameters of several HTSc materials [92], including the upper critical fields, B_{c2}, measured parallel ($B_{c2}{}^{ab}$) and perpendicular ($B_{c2}{}^{c}$) to the (a,b)-plane.

Table 1 Superconducting parameters of several HTSc compounds. Data were collected from Ref. [69]

Cuprate	T_c (K)	ξ_{ab} (nm)	ξ_c (nm)	λ_{ab} (nm)	λ_c (nm)	$B_{c2}{}^{ab}$ (T)	$B_{c2}{}^{c}$ (T)	κ_{ab}
LSCO	38	3.3	0.25	200	2000	80	15	61
NCCO	25	7–8	0.15	120	2600	7	–	15
YBCO	92	1.3	0.2	145	600	150	40	115
Bi-2212	95	1.5	0.1	180	700	120	30	120
Bi-2223	110	1.3	0.1	200	1000	250	30	150
Tl-1223	133	1.4	0.1	150	–	160	–	110
Hg-1223	134	1.3	0.2	177	3000	190	–	136

The data of Fig. 18 and of Table 1 now reveal that applications operating at 77 K demand the use of the RE-123 compounds, whereas tapes or wires of the BSCCO family require to be cooled down to at least 20 K [93], if not to 4.2 K, where the so much higher B_{c2} is justifying their use even as inset coils into conventional Nb_3Sn magnets.

To discuss the problems appearing for the use of RE-123 in applications, it is essential to have a closer look on the characteristic microstructure of the superconducting samples. When preparing HTSc superconductors in a solid-state reaction, the resulting material will be polycrystalline consisting of superconducting grains with typical sizes ranging between 1 and 20 μm. When sending electric currents through such samples, one immediately realizes that only small currents can be sent without showing a too high resistance. The problems are due to the grain boundaries (GBs), which act as weak links for the current flow. Thus, to avoid the GBs, texture of the material is required, which is very demanding for the sample preparation, and lot of work in the field of HTSc was devoted to develop preparation techniques to achieve a good texture [76–78].

A first stage of microstructures is presented in Fig. 19, where single crystals and melt-textured RE-123 samples are shown [94–96]. The typical structure is caused by the twin boundaries, which appear in the sample preparation when cooling down the sample from close to the melting temperature. In this stage, RE-123 has the tetragonal crystal structure and is converted to orthorhombic by oxygen uptake, which is done

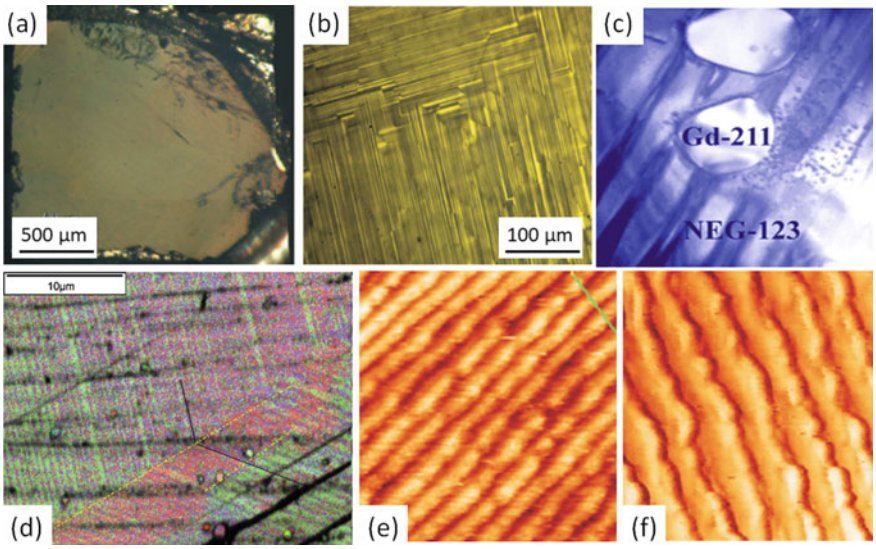

Fig. 19 Various microstructures of YBCO samples. **a** Typical *RE*-123 single crystal, optical image [91]. **b** Polarization image of an (*a,b*)-surface revealing the twin structure [91]. **c** Twins and embedded Gd-211 particles in the superconducting matrix of NEG-123. **d** Analysis of the twin structure by means of EBSD. (Image (**d**) was reproduced from Ref. [95]). **e** Nanostripes of SmBCO showing a regular pattern and **f** irregular pattern [91]

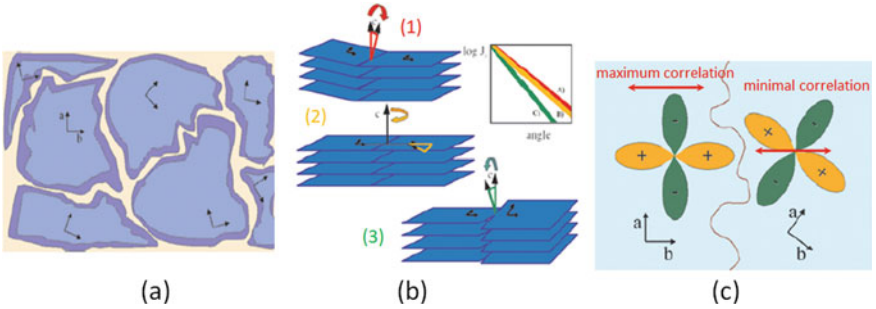

Fig. 20 Illustrations to the GB problem of HTSc. **a** Gives a schematic view of a polycrystalline sample with grains of different orientations in blue. The border area of the grain (violet) can be oxygen-depleted. **b** Shows possible grain boundaries, (1) tilted, (2) rotated in plane and (3) distorted. The small graph indicates that currents are lowest for case (3). **c** Shows the cancelling effect as a reason for the weak link effect of the GBs regarding the superconducting phase (*d*-wave-symmetry). Reproduced with permission from Ref. [88]

mostly in a separate oxygen-loading step. The twins are 90°-twins by interchanging the *a*- and *b*-axis of the material, and form twin domains [90]. The twin boundaries are guiding the vortex motion in a superconducting sample, as moving along the twins is easier as crossing them. The border area of such twin domains is also a weak section, allowing penetrating flux to rush along there [97]. Thus, the twin pattern does have an influence on the magnetic properties of the RE-123 compounds. The nanostripes of some RE-BCO compounds are observable using AFM or STM at ambient conditions [96] and are created during the growth of the superconducting matrix, especially in the melt-growth techniques, which are applied to grow bulk samples. Also these nanostripes can influence the vortex motion as demonstrated in dedicated transport measurements [98].

The basic character of the GBs in all HTSc materials was topic of many research reports in the literature, and the output is summarized in [76–78]. Figure 20 gives a short overview of the GB problem. In (a), a typical polycrystalline sample is sketched schematically. The grains may have different orientations, and their border areas may be oxygen-depleted. Furthermore, some impurities or secondary phases may be found along the GBs. (b) shows three cases (1–3) of GBs, and the small inset indicates that the situation (3) is the worst for a transport current. Finally, (c) illustrates a possible explanation for the weak link character regarding the superconducting phase in each grain (*d*-wave character). The interaction between the two different phases reduces the currents through the GB as indicated; maximum correlation yields the highest current through the boundary, the minimal configuration the lowest.

Figure 21 presents a magneto-optical (MO) analysis of the flux penetration along GBs with different angles, which were obtained in YBCO thin films, deposited on respective bicrystal substrates [99]. The MO images demonstrate clearly that flux can easily rush along a GB if the misorientation is higher than 5°. Thus, it is obvious that achieving a good texture is essential to reach high critical current densities in HTSc samples.

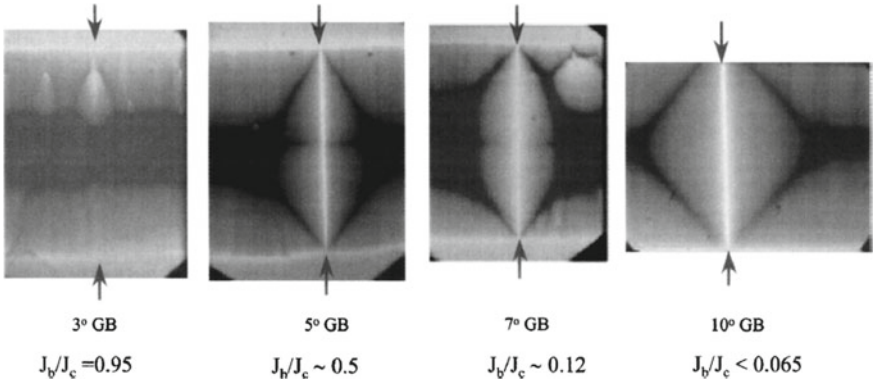

Fig. 21 Magneto-optic observations of flux penetration a thin film along a GB with different angles. The current ratio, J_b/J_c, strongly reduces on increasing the angle. Reproduced with permission from Ref. [99]

4 HTSc Cuprates and Applications

Several new preparation techniques and approaches were developed since the discovery of the HTSc, with the main demand to achieve a good sample texture. Figure 22 presents several samples for applications of the RE-123 family. Image

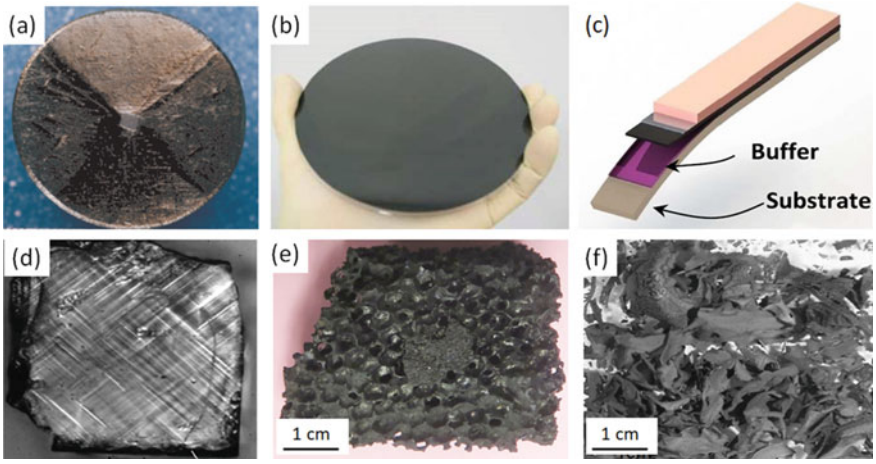

Fig. 22 Typical samples of the RE-123 HTSc family for applications. **a** Melt-textured Gd-123 bulk (see the seed crystal in the sample center) [91]. **b** 15 cm-diameter YBCO thin film (Ceraco) [103], **c** Sketch of YBCO coated conductor [104], **d** Large twinned single crystal of NdBCO for basic research [105], **e** Superconducting YBCO foam (details described in open accessed Ref. [106]), and **f** YBCO nanofiber mat [28]. Images c, d, and f were reproduced from Refs. [104, 105], and [28], respectively

(a) shows a melt-textured, bulk RE-123 sample with a typical diameter of 2 cm for laboratory use. This type of sample processing was discussed in Refs. [100, 101]. Nowadays, batch-processed samples with diameters up to 10 cm can be fabricated [102]. (b) presents a YBCO thin film sample with a diameter of 15 cm, fabricated by Ceraco [103]. (c) shows an YBCO coated conductor in uncovered state. The YBCO thick film is prepared by CVD on a metal substrate, requiring some intermediate buffer layers to get a suitable base for the growth of YBCO [104]. (d) presents a large, twinned single crystal of NdBCO [105] which is interesting for basic research, and (e) gives a superconducting, open-cell porous YBCO foam [106] and finally, (f) a solution-spun YBCO nanofiber mat [28, 107].

The last two sample types are porous materials, the advantages of which were discussed in Refs. [107, 108, 109]; the materials are light weight and exhibit improved oxygenation and cooling properties, avoiding the problems appearing when trying to increase to sample diameters further.

Figure 23 shows samples for applications from the BSCCO HTSc family. As it was most straightforward to use the powder-in-tube technique from the Nb_3Sn-fabrication also for HTSc, the Bi-2223 compound turned out to be more useful in tape form as YBCO due to the easier alignment of the elongated Bi-2223 grains during rolling and wire drawing. Tapes of this type could reach 1 km in length (a), and were thus the first choice for demonstrators for energy applications [110]. Bi-2212 wires

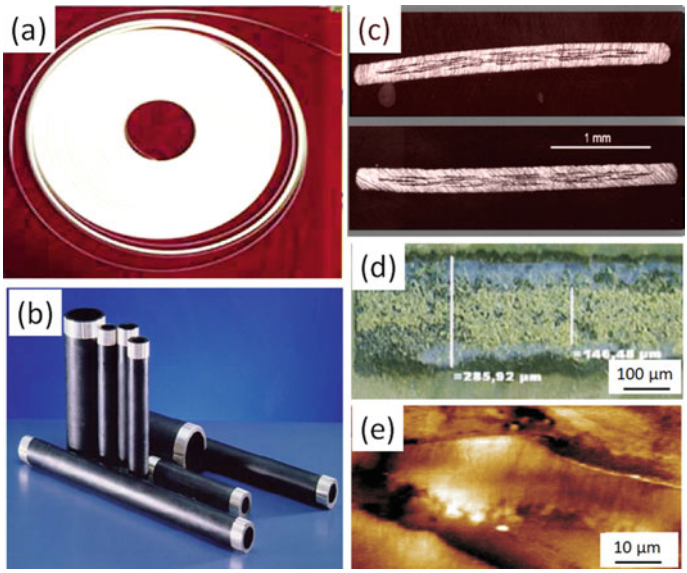

Fig. 23 Samples and microstructures of the BSCCO family for applications. **a** First-generation silver-sheathed Bi-2223 tape [110], **b** melt-cast Bi-2212 samples for current leads (Nexans, [112]). **c** presents the cross-sections of multifilamentary Bi-2223 tapes, image from [113], **d** an extracted filament, and **e** an AFM topography image of the Bi-2223 grains. Images (**d**) and (**e**) were reproduced from Ref. [114]

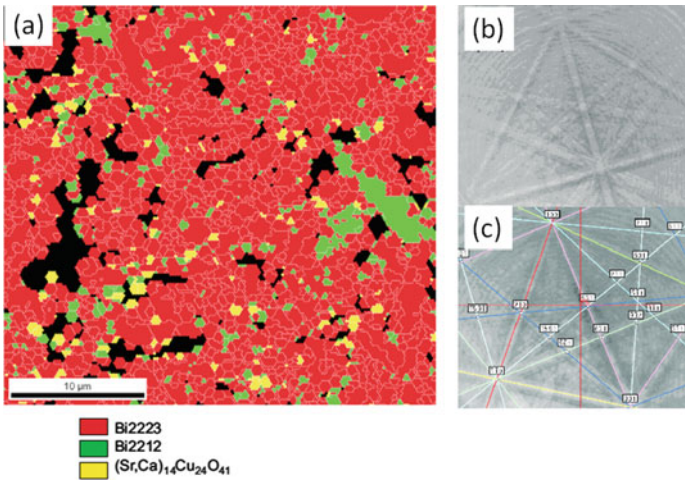

Fig. 24 **a** EBSD-analysis of a section of a Bi-2223 tape, showing the phase map (color code below the map) together with the EBSD-detected GBs (marked white). Reproduced with permission from Ref. [116]. **b** Kikuchi pattern of the Bi-2223 phase and **c** indexation

were also fabricated in the same way for high-field applications at low temperatures [111], and melt-cast Bi-2212 samples (b) could be used for current leads [112]. Image (c) gives two cross-sections of Bi-2223 multifilamentary tape [113], (d) presents an optical image of an extracted filament and an AFM topography image [114].

Here, it must be mentioned that the microstructure of the HTSc samples requires nanoengineering, as the flux pinning sites should be of a size comparable to 2ξ, and thus, the size of the optimum flux pinning sites is about 10 nm [61, 115]. The consequence of this is that also the required analysis techniques are pushed to their limits. A typical example for a dedicated sample analysis is presented in Fig. 24 as performed in [116].

The electron backscatter diffraction (EBSD) technique developed into a routine tool to investigate the nanostructures of ceramic materials during the development of the HTSc conductors and could thus deliver important contributions to it [116–118]. The main problem for the fabrication of HTSc wires or tapes is now to maintain control on the nanoscale while preparing meter-long materials. All the efforts made are summarized in [119–123]. Thus, the preparation of HTSc samples for applications is still a demanding challenge for further research and development.

5 Conclusion

The present chapter has shown the crystal structures of all the important HTSc family members and discussed the respective properties due to the nature of being ceramic oxidic materials. Thus, effects of doping, oxygen-loading and –depletion play an

important role for the superconducting performance of the cuprate HTSc samples. The cuprate HTSc are still the only superconducting materials enabling applications of superconductivity at 77 K with liquid nitrogen as coolant. Samples for applications come mainly from the RE-123 family and of the BSCCO family, whereas the TlBCCO and HgBCCO families are not considered for applications despite their much higher T_c-values. The main reason for this is the grain boundary problem, from which all cuprate HTSc suffer. This also lines out that achieving good sample textures in the sample fabrication is an essential task to obtain high critical current densities demanded for the applications. To do so, not only the preparation techniques had to be developed or to be improved, but also the required analysis and characterization techniques required further development in order to enable nanoengineering of the flux pinning sites within the HTSc materials.

All the images of crystal structures were prepared using the software VESTA [124].

References

1. A.V. Narlikar, *Superconductors* (Oxford University Press, Oxford, U.K., 2014)
2. W. Buckel, R. Kleiner, *Supraleitung. Grundlagen und Anwendungen*, 7th edn (Wiley-VCH, Weinheim, 2013)
3. K.H. Bennemann, J.B. Ketterson (eds.), *Superconductivity* (Springer, Berlin, Heidelberg, Germany, 2008)
4. K.A. Müller, J.G. Bednorz, Possible high T_c superconductivity in the Ba-La-Cu–O system. Z. Phys. B **64**, 189–193 (1986)
5. R. Hazen, *Superconductors: The Breakthrough* (Summit Books, N.Y., USA, 1988)
6. H. Takagi, S. Uchida, K. Kitazawa, S. Tanaka, High-T_c Superconductivity of La-Ba-Cu Oxides. II.—Specification of the Superconducting Phase. Jpn. J. Appl. Phys. **26**, L123–L124 (1987)
7. M.K. Wu, J.R. Ashburn, C.J. Torng, P.H. Hor, R.L. Meng, L. Gao, Z.J. Huang, Y.Q. Wang, C.W. Chu, Superconductivity at 93 K in a new mixed-phase Y-Ba-Cu-O compound system at ambient pressure. Phys. Rev. Lett. **58**, 908–910 (1987)
8. C.W. Chu, P.H. Hor, R.L. Meng, L. Gao, Z.J. Huang, Y.Q. Wang, Evidence for superconductivity above 40 K in the La-Ba-Cu-O compound system. Phys. Rev. Lett. **58**, 405–407 (1987)
9. H. Maeda, Y. Tanaka, M. Fukutomi, T. Asano, A new high-T_c oxide superconductor without a rare earth element. Jpn J. Appl. Phys. **27**, L209–L210 (1988)
10. H.W. Zandbergen, Y.K. Huang, M.J.V. Menken, J.N. Li, K. Kadowaki, A.A. Menovsky, G. van Tendeloo, S. Amelinckx, Electron microscopy on the $T_c = 110$ K (midpoint) phase in the system Bi_2O_3–SrO–CaO–CuO. Nature **332**, 620–623 (1988)
11. Z.Z. Sheng, A.M. Hermann, Bulk superconductivity at 120 K in the Tl–Ca/Ba–Cu–O system. Nature **332**, 138–139 (1988)
12. D. Tristan Jover, R.J. Wijngaarden, R. Griessen, E.M. Haines, J.L Tallon, R.S. Liu, Pressure dependence of the superconducting critical temperature of $Tl_2Ba_2Ca_2Cu_3O_{10+y}$ and $Tl_2Ba_2Ca_3Cu_4O_{12+y}$ up to 21 GPa. Phys. Rev. B. **54**, 10175–10185 (1996)
13. A. Iyo, Y. Tanaka, Y. Ishiura, M. Tokumoto, K. Tokiwa, T. Watanabe, H. Ihara, Study on enhancement of T_c ($\geqslant$130 K) in $TlBa_2Ca_2Cu_3Oy$ superconductors. Supercond. Sci. Technol. **14**, 504–510 (2001)
14. S.N. Putilin, E.V. Antipov, O. Chrnaissem, M. Marezio, Superconductivity at 94 K in $HgBa_2Cu0_{4+\delta}$. Nature **362**, 226–228 (1993)

15. A. Schilling, M. Cantoni, J.D. Guo, H.R. Ott, Superconductivity above 130 K in the Hg–Ba–Ca–Cu–O system. Nature **363**, 56–58 (1993)
16. K.A. Lokshin, D.A. Pavlov, S.N. Putilin, E.V. Antipov, D.V. Sheptyakov, A.M. Balagurov, Enhancement of T_c in $HgBa_2Ca_2Cu_3O_{8+\delta}$ by fluorination. Phys. Rev. B **63**, 064511 (2001)
17. L. Gao, Superconductivity up to 164 K in $HgBa_2Ca_{m-1}Cu_mO_{2+2+\delta}$ (m = 1, 2, and 3) under quasihydrostatic pressures. Phys. Rev. B **50**, 4260–4263 (1994)
18. A.P. Drozdov, M.I. Eremets, I.A. Troyan, V. Ksenofontov, S.I. Shylin, Conventional superconductivity at 203 kelvin at high pressures in the sulfur hydride system. Nature **525**, 73–76 (2015)
19. A.P. Drozdov, P.P. Kong, V.S. Minkov, S.P. Besedin, M.A. Kuzovnikov, S. Mozaffari, L. Balicas, F.F. Balakirev, D.E. Graf, V.B. Prakapenka, E. Greenberg, D.A. Knyazev, M. Tkacz, M.I. Eremets, Superconductivity at 250 K in lanthanum hydride under high pressures. Nature **569**, 528–533 (2019)
20. A.V. Narlikar (ed.), *Frontiers in Superconducting Materials* (Springer, Berlin, Heidelberg, Germany, 2005)
21. Y. Tokura, H. Takagi, S. Uchida, A superconducting copper oxide compound with electrons as the charge carriers. Nature **337**, 345–347 (1989)
22. J.T. Markert, M.B. Maple, High temperature superconductivitity in Th-doped Nd_2CuO_{4-y}. Solid State. Commun. **70**, 145–147 (1989)
23. B. Seeber (ed.), *Handbook of Applied Superconductivity* (IOP Publishing, Bristol, UK, 1999)
24. D.A. Cardwell, D.S. Ginley (eds.), *Handbook of Superconducting Materials* (CRC Press, London, U.K., 2002)
25. P. Seidel (ed.), *Applied Superconductivity* (Wiley-VCH, Weinheim, Germany, 2015)
26. E.S. Reddy, G.J. Schmitz, Superconducting foams. Supercond. Sci. Technol. **15**, L21–L24 (2002)
27. M.R. Koblischka, S. Pavan Kumar Naik, A. Koblischka-Veneva, M. Murakami, D. Gokhfeld, E.S. Reddy, G.J. Schmitz, Superconducting YBCO foams as trapped field magnetis. Materials **12**, 853 (2019)
28. X.L. Zeng, T. Karwoth, M.R. Koblischka, U. Hartmann, D. Gokhfeld, C. Chang, T. Hauet, Analysis of magnetization loops of electrospun nonwoven superconducting fabrics. Phys. Rev. Mater. **1**, 044802 (2017)
29. M. Rotta, L. Zadorosny, C.L. Carvalho, J.A. Malmonge, I.F. Malmonge, R. Zadorosny, YBCO ceramic nanofibers obtained by the new technique of solution blow spinning. Ceram. Int. **42**, 16230–16234 (2016)
30. L. Duband, Space cryocooler development. Phys. Proc. **67**, 1–10 (2015)
31. D. van Delft, P.H. Kes, The discovery of superconductivity. Phys. Today **63**, 38–43 (2010)
32. J.L. Tallon, Oxygen in high-T_c cuprate superconductors, in *Frontiers in Superconducting Materials*, ed. by A.V. Narlikar (Springer, Berlin, Heidelberg, Germany, 2005)
33. Ø. Fischer, M. Kugler, I. Maggio-Aprile, C. Berthod, Scanning tunneling spectroscopy of high-temperatur superconductors. Rev. Mod. Phys. **79**, 353–419 (2007)
34. A. de Visser, Magnetic field–boosted superconductivity. Phys. Today **73**, 44–50 (2020)
35. A. Koblischka-Veneva, N. Sakai, S. Tajima, M. Murakami, YBCO, in *Handbook of Superconducting Materials*, ed. by D.A. Cardwell, D.S. Ginley (CRC Press, Boca Raton, USA, 2002)
36. D.C. Larbalestier, A. Gurevich, D.M. Feldmann, A. Polyanskii, High-T_c superconducting materials for electric power applications. Nature **414**, 368–377 (2001)
37. C.W. Chu, P.H. Hor, R.L. Meng, L. Gao, Z.J. Huang, Superconductivity at 52.5 K in the lanthanum-barium-copper-oxide system. Science **235**, 567–569 (1987)
38. D.A. Cardwell, N. Hari Babu, Improved magnetic flux pinning in bulk RE(BCO) superconductors. AIP Conf. Proc. **986**, 543–550 (2008)
39. R.J. Cava, B. Batlogg, C.H. Chen, E.A. Rietman, S.M. Zahurak, D. Werder, Oxygen stoichiometry, superconductivity and normal state properties of $YBa_2Cu_3O_{7-\delta}$. Nature **329**, 423–425 (1987)

40. H.F. Poulsen, N.H. Andersen, J.V. Andersen, H. Bohr, O.G. Mouritsen, Relation between superconducting transition temperature and oxygen ordering in $YBa_2Cu_3O_{6+x}$. Nature **349**, 594–596 (1991)
41. N.H. Andersen, M. von Zimmermann, T. Frello, M. Käll, D. Mønster, P.-A. Lindgard, J. Madsen, T. Niemöller, H.F. Poulsen, O. Schmidt, J.R. Schneider, T. Wolf, P. Dosanjh, R. Liang, W.N. Hardy, Superstructure formation and the structural phase diagram of $YBa_2Cu_3O_{6+x}$. Physica C **317–318**, 259–269 (1999)
42. P. Diko, M. Kaňuchová, X. Chaud, P. Odier, X. Granados, X. Obradors, Oxygenation mechanism of TSMG YBCO Bulk Superconductor. J. Phys. Conf. Ser. **97**, 012160 (2008)
43. I. Maggio-Aprile, C. Renner, A. Erb, E. Walker, O. Fischer, Direct vortex lattice imaging and tunneling spectroscopy of flux lines on $YBa_2Cu_3O_{7-\delta}$. Phys. Rev. Lett. **75**, 2754–2757 (1995)
44. M. Maki, T. Nishizaki, K. Shibata, T. Sasaki, N. Kobayashi, Low temperature STM/STS of high-T_c superconductors. Physica C **357–360**, 291293 (1995)
45. G. Blatter, M.V. Feigel'man, V.B. Geshkenbein, A.I. Larkin, V.M. Vinokur, Vortices in high-temperature superconductors. Rev. Mod. Phys. **66**, 1125–1388 (1994)
46. M.R. Koblischka, M. Murakami, Pinning mechanisms in bulk high-T_c superconductors. Supercond. Sci. Technol. **13**, 738–744 (2000)
47. M. Jirsa, L. Půst, D. Dlouhy, M.R. Koblischka, Fishtail shape in the magnetic hysteresis loop for superconductor: Interplay between different pinning mechanisms. Phys. Rev. B **55**, 3276–3284 (1997)
48. A. Erb, J.-Y. Genoud, F. Marti, M. Däumling, E. Walker, R. Flükiger, Reversible suppression of the so-called fishtail effect in ultra pure single crystals of $YBa_2Cu_3O_{7-\delta}$ achieved by proper oxygenation. J. Low Temp. Phys. **105**, 1023–1028 (1996)
49. M. Däumling, J.M. Seuntjens, D.C. Larbalestier, Oxygen-defect flux pinning, anomalous magnetization and intra-grain granularity in $YBa_2Cu_3O_{7-\delta}$. Nature **346**, 332–335 (1990)
50. P.H. Hor, R.L. Meng, Y.Q. Wang, L. Gao, Z.L. Huang, J. Bechtold, K. Forster, C.W. Chu, Superconductivity above 90 K in the square-planar compound system $ABa_2Cu_3O_{6+x}$ with A = Y, La, Nd, Sm, Eu, Gd, Ho. Er and Lu. Phys. Rev. Lett. **58**, 1891–1894 (1987)
51. H.A. Blackstead, J.D. Dow, Implications of superconductivity of $PrBa_2Cu_3O_7$. Solid State Commun. **115**, 137–140 (2000)
52. P. Pęczkowski, P. Zachariasz, C. Jastrzębski, J. Piętosa, E. Drzymała, Ł Gondek, On the superconductivity suppression in $Eu_{1-x}Pr_xBa_2Cu_3O_{7-\delta}$. Materials **14**, 3503 (2021)
53. M. Erbe, P. Cayado, W. Freitag, K. Ackermann, M. Langer, A. Meledin, J. Hänisch, B. Holzapfel, Comparative study of CSD-grown REBCO films with different rare earth elements: processing windows and T_c. Supercond. Sci. Technol. **33**, 094002 (2020)
54. H.S. Chauhan, M. Murakami, Temperature-controlled tailoring of J_c(B)-properties in the Nd-Ba-Cu–O system. Appl. Supercond. **6**, 169–174 (1998)
55. T. Saitoh, K. Segawa, K. Kamada, N. Sakai, T. Segawa, S.I. Yoo, M. Murakami, Microstructures and superconducting properties of melt processed (RE,RE')-Ba-Cu–O. Physica C **288**, 141–147 (1997)
56. M.R. Koblischka, M. Muralidhar, M. Murakami, Flux pinning in ternary $(Nd_{0.33}Eu_{0.33}Gd_{0.33})Ba_2Cu_3O_y$ melt-processed superconductors. Appl. Phys. Lett. **73**, 2351–2353 (1998)
57. M. Muralidhar, K. Suzuki, Y. Fukumoto, A. Ishihara, M. Tomita, Recent progress on batch processed large size LRE-123 bulk. Physica C **484**, 108–111 (2013)
58. Y. Shukunami, A. Yamashita, Y. Goto, Y. Mizoguchi, Synthesis of RE123 high-T_c superconductors with a high-entroy-alloy-type RE site. Physica C **572**, 1353623 (2020)
59. M.J. Kramer, A. Karion, K.W. Dennis, M. Park, R.W. Mc Callum, Enhanced superconductivity in $Nd_{1-x}Ba_{2-x}Cu_3O_{7-\delta}$ by low oxygen partial pressure annealing. J. Electron. Mater. **23**, 1117–1120 (1994)
60. M.R. Koblischka, Nanoengineering of flux pinning sites in high-T_c superconductors. Tsinghua Sci. Technol. **8**, 280–291 (2003)
61. M.R. Koblischka, A. Koblischka-Veneva, M. Murakami, Nanosized pinning sites in HTSc compounds. J. Supercond. **17**, 373–377 (2004)

62. P. Das, M.R. Koblischka, T. Wolf, P. Adelmann, U. Hartmann, T_c-dependence of energy gap and asymmetry of coherence peaks in $NdBa_2Cu_3O_{7-\delta}$ superconductors. Europhys. Lett. **84**, 47004 (2008)
63. W. Ting, N. Koshizuka, S. Tanaka, Highly stable surfaces of $NdBa_2Cu_3O_y$ single crystals. Appl. Phys. Lett. **72**, 2035–2037 (1998)
64. G. Deutscher, Coherence and single-particle excitations in the high temperature superconductors. Nature **397**, 410–412 (1999)
65. J.L. Tallon, D.M. Pooke, R.G. Buckley, M.R. Presland, F.J. Blunt, $R_2Ba_4Cu_7O_{15-\delta}$: A 92-K bulk superconductor. Phys. Rev. B **41**, 7220–7223 (1990)
66. J.-Y. Genoud, G. Triscone, A. Junod, J. Muller, Stability, superconducting and magnetic properties of $Y_2Ba_4Cu_7O_x$ annealed under high oxygen pressure. Physica C **235–240**, 443–444 (1994)
67. C. Michel, M. Hervieu, M.M. Borel, A. Grandin, F. Deslandes, J. Provost, B. Raveau, Superconductivity in the Bi-Sr-Cu–O system. Z. Phys. B **68**, 421–423 (1987)
68. S.A. Sunshine, T. Siegrist, L.F. Schneemeyer, D.W. Murphy, R.J. Cava, B. Batlogg, R.B. van Dover, R.M. Fleming, S.H. Glarum, S. Nakahara, J.J. Krajewski, S.M. Zahurak, J.V. Waszczak, J.H. Marshall, L.W. Rupp, Jr., W.F. Peck, Structure and physical properties of single crystals of the 84-K superconductor $Bi_{2.2}Sr_2Ca_{0.8}Cu_2O_{8+\delta}$. Phys. Rev. B **38**, 893–896 (1988)
69. A. Mourachkine, *High Temperature Superconductivity in Cuprates. The Non-linear Mechanism and Tunneling Measurements* (Kluwer, London, U.K., 2002)
70. P.N. Mikheenko, K.K. Uprety, S.X. Dou, BSCCO, in *Handbook of Superconducting Materials*, ed. by D.A. Cardwell, D.S. Ginley (CRC Press: Boca Raton, USA, 2002)
71. T. Fujii, I. Terasaki, T. Watanabe, A. Matsuda, In-plane anisotropy on the transport properties in the modulated Bi_2O_2-based conductors Bi-2212 and Bi-Sr-Co-O. Physica C **378–381**, 182–186 (2002)
72. T. Watanabe, T. Fujii, A. Matsuda, Crystal growth and anisotropic transport properties of high-T_c superconductors $Bi_2Sr_2Ca_{n-1}O_{2n+4+\delta}$ (n = 2, 3). arXiv:cond-mat/0401448v3 (2004)
73. K.M. Lang, V. Madhavan, J.E. Hoffman, E.W. Hudson, H. Eisaki, S. Uchida, J.C. Davis, Imaging the granular structure of high-T_c superconductivity in underdoped $Bi_2Sr_2CaCu_2O_{8+\delta}$. Nature **415**, 412–416 (2002)
74. A. Iyo, Y. Aizawa, Y. Tanaka, Y. Ishiura, M. Tokumoto, K. Tokiwa, T. Watanabe, and H. Ihara, High-pressure synthesis of $Tl_2BaCa_{n-1}Cu_nO_y$ (n = 3 and 4) with T_c =133.5 K (n = 3) and 127 K (n = 4). Physica C **357–360**, 324–328 (2001)
75. X. Chen, C. Gong, Dependence of the superconducting transition temperature on the type and number of CuO_2 layers in $Tl_2Ba_2Ca_{n-1}Cu_{n2n+4-y}$. Phys. Rev. B **59**, 4513–4523 (1999)
76. E. Bellingeri, R. Flükiger, TlBCCO, in *Handbook of Superconducting Materials*, ed. by D.A. Cardwell, D.S. Ginley (CRC Press: Boca Raton, USA, 2002)
77. S.E. Babcock, J.L. Vargas, Boundaries in the high-T_c superconductors. Annu. Rev. Mater. Sci. **25**, 193–222 (1995)
78. H. Hilgenkamp, J. Mannhart, Grain boundaries in high-T_c superconductors. Rev. Mod. Phys. **74**, 485–549 (2002)
79. J. Ayache, Grain boundaries in high temperature superconducting ceramics. Phil. Mag. **86**, 2193–2239 (2006)
80. R. Flükiger, R. Gladyshevskii, E. Bellingeri, Methods to produce Tl(1223) tapes with improved properties. J. Supercond. **11**, 23–26 (1998)
81. A. Sundaresan, H. Asada, A. Crisan, J.C. Nie, H. Kito, A. Iyo, Y. Tanaka, M. Kusunoki, S. Ohshima, Preparation of Tl-2212 and Tl-1223 superconductor thin films and their microwave surface resistance. IEEE Trans. Appl. Supercond. **13**, 2913–2916 (2003)
82. J. Schwartz, P.V.P.S.S. Sastry, TlBCCO, in *Handbook of Superconducting Materials*, ed. by D.A. Cardwell, D.S. Ginley (CRC Press: Boca Raton, USA, 2002)
83. U. Welp, G.W. Crabtree, J.L. Wagner, D.G. Hinks, Flux pinning and the irreversibility lines in the $HgBa_2CuO_{4+\delta}$, $HgBa_2CaCu_2O_{6+\delta}$ and $HgBa_2Ca_2Cu_3O_{8+\delta}$ compounds. Physica C **218**, 373–378 (1993)

84. Z.J. Huang, Y.Y. Xue, R.L. Meng, C.W. Chu, Irreversibility line of the $HgBa_2CaCu_2O_{6+\delta}$ high-temperature superconductors. Phys. Rev. B **49**, 4218–4221 (1994)
85. R. Hott, Material aspects of high temperature superconductors for applications, in *High Temperature Superconductivity 1-Materials*, ed. by A.V. Narlikar (Springer, Berlin, Germany, 2004)
86. M. Azuma, Z. Hiroi, M. Takano, Y. Bando, Y. Takeda, Superconductivity at 110 K in the infinite-layer compound $(Sr_{1-x}Ca_x)_{1-y}CuO_2$. Nature **356**, 775–776 (1992)
87. B. Stadlober, G. Krug, R. Nemetschek, R. Hackl, J.L. Cobb, J.T. Markert, Is $Nd_{2-x}Ce_xCuO_4$ a high-temperature superconductor? Phys. Rev. Lett. **74**, 4911–4914 (1995)
88. R. Hott, R. Kleiner, T. Wolf, G. Zwicknagl, Superconducting materials—a topical overview, in *Frontiers in Superconducting Materials*, ed. by A.V. Narlikar (Springer, Berlin, Heidelberg, 2005)
89. D. Lindner, Electron doped cuprates. https://guava.physics.uiuc.edu/~nigel/courses/569/Essays_Spring2006/files/Lindner.pdf. Accessed 22 Aug 2021
90. A. Gurevich, To use or not to use cool superconductors. Nat Mater. **10**, 255–259 (2011)
91. M.R. Koblischka, *Habilitation Thesis* (Saarland University, Saarbrücken, 2012)
92. J.R. Clem, Pancake vortices. J. Supercond. **17**, 613–629 (2004)
93. M.R. Koblischka, J. Sosnowski, Temperature-dependent scaling of pinning force data in Bi-based high-T_c superconductors. Eur. Phys. J. B **44**, 277–280 (2005)
94. M. Muralidhar, M.R. Koblischka, M. Murakami, Embedding of 211 particles in NEG-123 superconductors. Supercond. Sci. Technol. **12**, 555–562 (1999)
95. A. Koblischka-Veneva, M.R. Koblischka, Analysis of twin boundaries using the electron backscatter diffraction (EBSD) technique. Mat. Sci. Eng. B **151**, 60–64 (2008)
96. M.R. Koblischka, M. Winter, U. Hartmann, Nanostripe structures in $SmBa_2Cu_3O_x$ superconductors. Supercond. Sci. Technol. **20**, 681–686 (2007)
97. T. Schuster, M.R. Koblischka, H. Kronmüller, Magneto-optical imaging of Shubnikov phase. J. Alloy Comp. **195**, 483–490 (1993)
98. M.R. Koblischka, U. Hartmann, Evidence for a directed δT_c-type flux pinning by means of nanostripes in $(Sm_{0.33}Eu_{0.33}Gd_{0.33})Ba_2Cu_3O_y$ high-T_c superconductors. Europhys. Lett. **89**, 47002 (2010)
99. A.A. Polyanskii, A. Gurevich, A.E. Pashitski, N.F. Heinig, R.D. Redwing, J.E. Nordman, D.C. Larbalestier, Magneto-optical study of flux penetration and critical current densities in [001] tilt $YBa_2Cu_3O_{7-\delta}$ thin-film bicrystals. Phys. Rev. B **53**, 8687–8697 (1996)
100. M. Murakami (ed.), *Melt Processed High Temperature Superconductors* (World Scientific, Singapore, 1991)
101. R. Tournier, E. Beaugnon, O. Belmont, Processing of large $YBa_2Cu_3O_{7-x}$ single domains for current-limiting applications. Supercond. Sci. Tech. **13**, 886–896 (2000)
102. D.K. Namburi, Y. Shi, D.A. Cardwell, The processing and properties of bulk (RE)BCO high temperature superconductors: current status and future perspectives. Supercond. Sci. Technol. **34**, 053002 (2021)
103. Ceraco ceramic coating, https://www.ceraco.de. Accessed 22 Aug 2021
104. V. Solovyov, P. Farrell, Exfoliated YBCO filaments for second-generation superconducting cable. Supercond. Sci. Technol. **30**, 014006 (2017)
105. M. Jirsa, M.R. Koblischka, T. Higuchi, M. Murakami, Effect of twin planes in the magnetization hysteresis loops of $NdBa_2Cu_3O_7$ single crystals. Phys. Rev. B **58**, R14771–R14774
106. M.R. Koblischka, S. Pavan Kumar Naik, A. Koblischka-Veneva, M. Murakami, D. Gokhfeld, E.S. Reddy, G.J. Schmitz, Superconducting YBCO foams as trapped field magnets. Materials **12**, 853 (2019)
107. M.R. Koblischka, A. Koblischka-Veneva, Fabrication of superconducting nanowires using the template method. Nanomaterials **11**, 1970 (2021)
108. M.R. Koblischka, A. Koblischka-Veneva, Porous high-T_c superconductors and their applications. AIMS Mater. Sci. **5**, 1199–1213 (2018)
109. D.M. Gokhfeld, M.R. Koblischka, A. Koblischka-Veneva, High-porous superconductors: synthesis, investigations and perspectives. Phys. Met. Metall. **121**, 1026–1038 (2020). ((in Russian))

110. L. Xiao, D. Zheng, P. Zhang, L. Lin, Recent research activities of applied superconductivity in China. Available at: https://snf.ieeecsc.org/sites/ieeecsc.org/files/documents/snf/abstracts/ed3_XIAO-Presentation%20at%20ASC2016%20annotated_0.pdf. Accessed 01 Sept 2021
111. F. Kametani, J. Jiang, M. Matras, D. Abraimov, E.E. Hellstrom, D.C. Larbalestier, Comparison of growth texture in round Bi2212 and flat Bi2223 wires and its relation to high critical current density development. Sci. Rep. **5**, 8285 (2015)
112. J. Bock, F. Breuer, C.-E. Bruzek, N. Lallouet, M.O. Rikel, H. Walter, NEXANS activities and plans on HTS materials. High-performance Bi2212 tape and bulk conductors for magnet technology. Proc. WAMS 2004, 22–24.03.2004, Archamps, France. Available at: https://www.yumpu.com/en/document/read/46876933/here-accelerator-magnet-technology-home-page-cern. Accessed 01 Sept 2021
113. M.R. Koblischka, T.H. Johansen, H. Bratsberg, P. Vase, Study of flux entry and exit into Bi-2223 multifilamentary tapes. Supercond. Sci. Technol. **11**, 479–484 (1998)
114. A. Koblischka-Veneva, M.R. Koblischka, Surface preparation of high-T_c superconductors for MO-imaging, in *Magneto-optical imaging*. ed. by T.H. Johansen, D.V. Shantsev (Kluwer academic Publishers, Dordrecht, The Netherlands, 2004), pp. 242–246
115. M.R. Koblischka, A. Koblischka-Veneva, Investigation of melt-textured superconductors on the nanoscale. Mat. Sci. Eng. B **151**, 47–52 (2008)
116. A. Koblischka-Veneva, M.R. Koblischka, T. Qu, Z. Han, F. Mücklich, Texture analysis of monofilamentary, Ag-sheathed (Pb, $Bi_)2S_r2C_a2C_u3_Ox$ tapes by electron backscatter diffraction (EBSD). Physica C **468**, 174–182 (2008)
117. A. Koblischka-Veneva, M.R. Koblischka, J. Schmauch, Y. Wan, J. Qian, X. Yao, EBSD characterization of specific microstructures in RE-BCO superconductors. IEEE Trans. Appl. Supercond. **29**, 6800504 (2019)
118. A. Koblischka-Veneva, M.R. Koblischka, J. Schmauch, M. Murakami, Secondary phase particles in bulk, infiltration-growth processed YBCO investigated by transmission Kikuchi diffraction and TEM. Supercond. Sci. Technol. **33**, 034010 (2020)
119. R.M. Scanlan, A.P. Malozemoff, D.C. Larbalestier, Superconducting materials for large scale applications. Proc. IEEE **92**, 1639–1654 (2004)
120. S.R. Foltyn, L. Civale, J.L. MacManus-Driscoll, Q.X. Jia, B. Maiorov, H. Wang, M. Maley, Materials science challenges for high-temperature superconducting wire. Nature Mater. **6**, 631–642 (2007)
121. M. Eisterer, S.H. Moon, H.C. Freyhardt, Current developments in HTSC coated conductors for applications. Supercond. Sci. Technol. **29**, 060301 (2016)
122. J.H. Durrell, M.D. Ainslie, D. Zhou, P. Vanderbemden, T. Bradshaw, S. Speller, M. Filipenko, D.A. Cardwell, Bulk superconductors: a roadmap to applications. Supercond. Sci. Technol. **31**, 103501 (2018)
123. A. Bussmann-Holder, H. Keller, High-temperature superconductors: underlying physics and applications. Z. Naturforschung **75**, 3–14 (2020)
124. K. Momma, F. Izumi, VESTA 3 for three-dimnsional visualization of crystal, volumetric and morphology data. J. Appl. Crystallogr. **44**, 1272–1276 (2011)